

Simulated influence of carbon dioxide, orbital forcing and ice sheets on the climate of the Last Glacial Maximum

Andrew J. Weaver, Michael Eby, Augustus F. Fanning & Edward C. Wiebe

School of Earth and Ocean Sciences, University of Victoria, PO Box 3055, Victoria, British Columbia, V8W 3P6, Canada

A coupled atmosphere–ocean–sea-ice model is used to investigate the climate of the Last Glacial Maximum (~21,000 years ago) and the relative climate-forcing effects of atmosphere CO₂, the Earth's orbital parameters and ice-sheet albedo. Tropical temperatures are found to be ~2.2 °C less than today's—slightly colder than indicated by the CLIMAP palaeoclimate reconstruction. This result is consistent with a low to medium climate sensitivity to radiative perturbations. Temperatures are colder still in the northern North Atlantic region, owing to a weakening and shallowing of the thermohaline circulation. A sensitivity analysis suggests that changes in ocean circulation since the Last Glacial Maximum have not contributed directly to the global-mean temperature change since that time.

Early CLIMAP^{1,2} attempts to reconstruct sea surface temperature (SST) for the Last Glacial Maximum (LGM), around 21 kyr ago, have suggested that relative to the present, global SSTs were on average 1.7 °C cooler in August and 1.4 °C cooler in February. These reconstructions further suggested that tropical SSTs were similar to those of the present climate whereas in the North Atlantic, SSTs were much colder. Although recent alkenone evidence^{3–6} also supports tropical SSTs having been only slightly cooler at the LGM, additional evidence is contradictory. For example, coral records from Barbados⁷ and the southwest Pacific⁸, ice-core records from Peru⁹, noble-gas measurements in Brazil¹⁰ and ocean core records from the western equatorial Atlantic¹¹ suggest that LGM tropical temperatures were significantly below the present-day values.

Most previous modelling studies of the LGM have fallen into two categories. In the first, ocean-only models have been used in which surface forcing consists of restoring temperature and salinity to LGM reconstructions with specified atmospheric general circulation model (AGCM) LGM surface wind stress fields^{12–14}. The second class of studies involves the integration of AGCMs with either fixed SST or mixed-layer ocean models at the lower boundary^{15–19}. Many of these modelling studies have found tropical SSTs consistent with CLIMAP, although this often (but not always; see, for example, ref. 15) reflects the fact that CLIMAP data were used as a boundary condition. Webb *et al.*²⁰ on the other hand obtained relatively cool tropical SSTs using an AGCM in which present-day oceanic heat transports were maintained. They argued that reduced evaporation in the subtropics with present-day oceanic heat transport led to reduced water vapour in the atmosphere, and hence reduced absorption of outgoing longwave radiation. These workers also suggested that this cooling mechanism was amplified by other processes in the system.

Until recently, it has not been possible to run coupled atmosphere–ocean GCM experiments to equilibrium for LGM scenarios owing to the necessity of applying explicit flux adjustments to keep stable the present-day climate. Any meaningful comparison between the simulated present-day and LGM climates would require the use of the same flux adjustment in the LGM case. The use of flux adjustments is only valid for small perturbations away from the present climate, whereas the LGM clearly represents a large perturbation. A recent study²¹ did, however, use a coupled GCM

under LGM forcing, albeit for a short (15-year) integration by which time the deep ocean was still far from equilibrium. Here we use a coupled model of intermediate complexity, which does not employ explicit flux adjustments to the heat and freshwater air–sea flux fields. The ocean component of the coupled model is a three-dimensional GCM, whereas the atmospheric component is an energy–moisture balance model (EMBM). This analysis takes a different, yet complementary, approach to another recent modelling study²² where a zonally averaged ocean model was coupled to a simple dynamical atmospheric model with parametrized synoptic variability. Our focus will be on changes in the three-dimensional ocean circulation and its feedback on LGM climate. We will show that changes in ocean circulation do not contribute to the global LGM cooling, and that the resulting tropical SSTs are slightly colder than CLIMAP, consistent with alkenone data.

The model

The atmospheric component of our coupled model²³ consists of energy and moisture balance equations for heat and fresh water. Poleward heat and freshwater transport are parametrized through Fickian diffusion, and precipitation is assumed to occur when the relative humidity reaches greater than 85%. Although the EMBM does not retain any explicit dynamics, a wind feedback parametrization is employed. During the spin-up to equilibrium, monthly climatological wind-stress fields were used at the ocean surface²⁴. Wind speeds were also derived from these fields²³ for use in the latent and sensible heat flux parametrizations at the air–sea interface. In the LGM experiments, perturbations of annual mean sea-level pressure away from the present-day equilibrium allowed for the calculation of anomalous geostrophic (frictional near the Equator) winds which were then rotated and contracted to yield wind stress/speeds. These in turn were added to the present-day fields²⁵. This approach therefore leads to a first-order approximation of atmospheric circulation feedbacks in response to changing surface air temperature (SAT) and humidity and hence sea-level pressure fields.

A thermodynamic sea-ice model²⁶ and a parametrization of water vapour/planetary longwave feedbacks²⁷ were also included in the model. Ice albedo feedbacks were incorporated, whenever sea ice was present and whenever the air temperature over land was below

−10 °C, by locally reducing the latitudinal profile of the co-albedo by 0.1 (ref. 28). In the LGM experiment, we also used this local co-albedo reduction at all land points where ice sheets were thought to be present²⁹. The ocean component of the coupled model is based on the GFDL model³⁰ as discussed in ref. 31. Precipitation over land was assumed to instantaneously return to the ocean via one of 21 river drainage basins (Fig. 1a). The coupled model has 3.75° zonal, and 1.8555° meridional, resolution with 19 vertical levels in the ocean.

The only differences between the LGM experiments and the present-day experiments are imposed changes in orbital parameters, atmospheric CO₂ concentrations and the presence of ice sheets (via an albedo feedback). The orbital parameters were set to values appropriate³² for 21 kyr ago and an atmospheric CO₂ concentration of 200 p.p.m. (compared with 350 p.p.m. for the present climate) was used. This CO₂ concentration was converted to a radiative forcing according to ref. 33 whereby a doubling of CO₂

leads to a radiative forcing of 4 W m^{−2}, translating to a radiative forcing of −3.2 W m^{−2} for the LGM. In our model, the equilibrium response for CO₂ doubling is a 3 °C increase in global-mean SAT so that its climate sensitivity is 0.75 °C W^{−1} m².

Simulations of the LGM and the present day

Four sets of simulations (experiments) were performed, with each set differing only in the river mask (drainage basins) that was used in the region around the North Atlantic. The reason for this sensitivity study will be apparent later. At this stage we address the results from the first suite of experiments (model 1) with a river mask (Fig. 1a) that leads to the most realistic representation of the present-day thermohaline circulation.

The first experiment in the model 1 suite was an integration of the model to equilibrium under present-day orbital and CO₂ forcing. In the North Atlantic, about 16 Sv of deep water formed at high latitudes with about 8 Sv being exported to the Southern Ocean

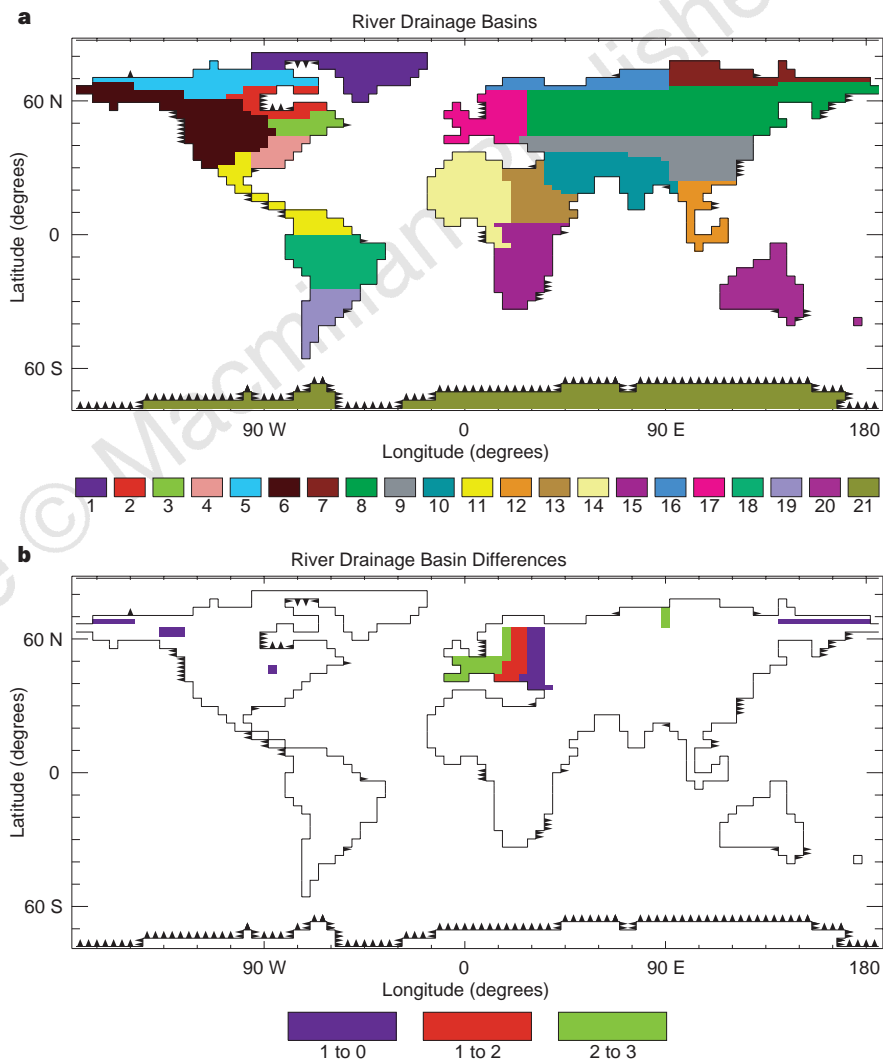


Figure 1 River drainage basins. **a**, Drainage basins for the 21 different areas defined. The numbers in the colour key refer to the following river basins: (1), Greenland; (2), Hudson Bay; (3), St Lawrence; (4), Mississippi; (5), Mackenzie; (6), Columbia; (7), Lena; (8), Amur; (9), Yangtze-Yellow; (10), Ganges; (11), Panama; (12), Mekong; (13), Nile; (14), Congo; (15), Lumpapa-Zambezi; (16), Yenesei-Ob; (17), Rhine; (18), Amazon; (19), La Plata; (20), Murray; (21), Antarctica. **b**, Changes made to the drainage basins between model 1 (the control) and models 0, 2 and 3. The dark blue area indicates changes between model 1 and model 0. These involved an expansion of the Rhine catchment area with reductions to both the Yangtze-

Yellow and Amur basins. In addition, small diversions were made from the Amur to the Lena, the Columbia to the St Lawrence, and the Columbia to the Mackenzie. The red indicates the changes between model 2 and model 1 which involved a reduction in the Rhine catchment area via an expansion of the Yangtze-Yellow and Amur basins. The green indicates further changes from model 2 to model 3. Here the Rhine catchment area is still further reduced with the Amur basin expanding more broadly westward. The arrows in **a** and **b** indicate discharge points for the particular drainage basin.

above 3,000 m depth (Fig. 2a). The deep Atlantic, south of about 30° N, is filled with Antarctic Bottom Water (AABW) formed in the Weddell and Ross seas. In the second experiment, the atmospheric CO₂ level was set to 200 p.p.m. and orbital parameters for 21 kyr ago were used. In addition, an ice-sheet albedo feedback was included wherever ice sheets were present in the reconstruction of ref. 29. The first important finding from our analysis is the weakening and shallowing, but not collapse, of the conveyor in the North Atlantic, and the enhanced intrusion there of AABW (Fig. 2b). The actual location of North Atlantic Deep Water (NADW) formation did not change and North Pacific Intermediate Water (NPIW) did not intensify, both in contrast with the results of ref. 22. In fact, we found a 50% reduction in NPIW formation (from 2.2 Sv to 1.1 Sv)

in our LGM climate. This discrepancy may lie in the fact that a zonally averaged ocean model with coarse meridional resolution (10°) was used in ref. 22. It is unlikely that the processes involved in the formation of NPIW (overflow from the Sea of Okhotsk and subsequent mixing of Oyashio waters with overlying Kuroshio waters in the Kuroshio extension) are well resolved in either of our models.

Associated with this thermohaline weakening and shallowing is a reduction in the heat transport in the North Atlantic (Fig. 2c). The results shown in Fig. 2c are in contrast with those in ref. 20 where it was assumed that ocean heat transport did not change in the LGM. The Atlantic heat transport curve in Fig. 2c has reduced everywhere in the North Atlantic (and subsequently the Northern Hemisphere). This was compensated for by an increase in the heat transport in the Southern Hemisphere.

The SST difference (Fig. 3a) is in excellent agreement with alkenone reconstructions^{3–6,34–36}. In particular, our tropical SST results are colder than those of CLIMAP^{1,2}, consistent with alkenone reconstructions^{3–6}, but not as cold as the bore-hole, coral and other data mentioned earlier^{7–11}. Model results reveal annual and global mean SST cooling of ~2.3 °C, with ~2.0–3.4 °C in the tropical Atlantic and ~2.0 °C in the tropical Indian oceans. In the North Atlantic the signal is amplified, with up to 6.3 °C cooling associated with a weakening and shallowing of the conveyor. The Pacific Ocean shows the greatest variance across the basin, with western tropical Pacific SSTs only about 1.9 °C cooler than today and eastern tropical Pacific SSTs as much as 3.1 °C cooler than today, suggesting that LGM Pacific SSTs are similar to permanent La Niña conditions.

The SAT difference (Fig. 3b–d) shows pronounced cooling around the region of the North Atlantic due to a weakening and shallowing of the conveyor, the southward expansion of sea ice and the subsequent sea–ice albedo feedback there. Averaged over the globe, the LGM experiment cooling is 3.2 °C, with more intense cooling in the Northern Hemisphere (where there is also more land) than in the Southern Hemisphere, yielding a pronounced asymmetry about the Equator. Cooling of 3.2 °C is slightly less than found in some AGCM studies^{16–18}, although it is similar to the amount found in others^{37,38}. In the Northern Hemisphere maximum winter-mean cooling of 14.4 °C is found in the North Atlantic; this weakens to about 6.8 °C in the summer. In the Southern Hemisphere, the seasonal-mean variation in maximum cooling over Antarctica (near the Ross Sea) ranges from 12.9 °C in winter to 5.7 °C in summer (Fig. 3c, d). The sea-ice distribution in the LGM experiment (solid line in Fig. 3c–d) bears reasonable agreement with various reconstructions^{39,40}. Of particular importance is the result that most of the North Atlantic is ice free when averaged over the summer months⁴¹.

To facilitate a detailed comparison between observed (CLIMAP^{1,2}) and model SST estimates, we first subtract the CLIMAP present-day reconstruction from the CLIMAP LGM reconstruction, for the month of February (winter) and again for the month of August (summer). We then compute the SST difference between our modelled LGM and present-day experiments for February and then for August. Finally, we subtract the observational difference field from our model difference field. In both the summer (Fig. 4a) and the winter (Fig. 4b), we find significantly more cooling in the subtropical North and South Pacific and Atlantic—with the exception of the subtropical North Atlantic, these are regions where CLIMAP data suggests modest LGM warming. The maximum Northern Hemisphere winter differences are 5.8 °C, 4.8 °C, 2.4 °C and 2.6 °C in the North Pacific, South Pacific, North Atlantic and South Atlantic subtropical gyres, respectively. These increase in the Northern Hemisphere summer to 6.8 °C, 3.1 °C and 3.3 °C in the South Pacific, North Atlantic and South Atlantic, respectively and decrease to 5.7 °C in the North Pacific. Our North Atlantic is also persistently less cool than CLIMAP, and our Southern Ocean has a more rich zonal structure.

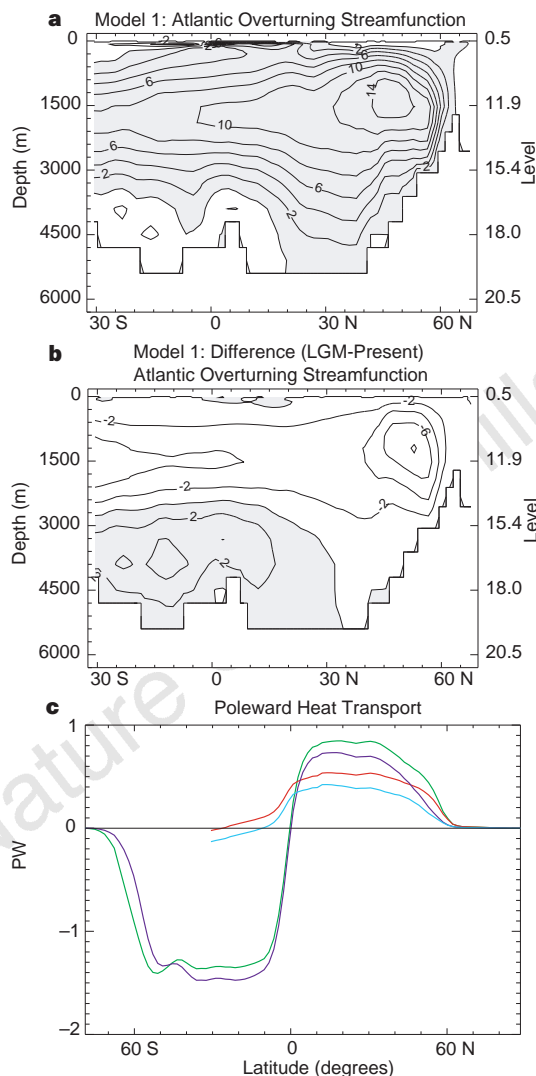


Figure 2 Present-day and LGM conveyor and poleward heat transport. **a**, Meridional overturning streamfunction in the Atlantic Ocean (contours, in Sv; 1 Sv = 10⁶ m³ s⁻¹) for the present-day equilibrium. **b**, Difference (contours, in Sv) between the LGM and the present-day meridional overturning in the Atlantic Ocean. The contour interval in **a** and **b** is 2 Sv, and clockwise circulation is shaded. **c**, Poleward heat transport in PW (1 PW = 10¹⁵ W) from the present-day and LGM experiments. The green and red lines represent the present-day global and Atlantic heat transports, respectively. The corresponding LGM curves are given by the purple and blue lines, respectively. The present-day heat transports are weaker than observational estimates, a feature which is common in coarse-resolution ocean GCMs which do not well represent narrow, intense western boundary currents. The model level corresponding to the depth is given on the right-hand y-axis.

Along the equatorial band in the Northern Hemisphere winter, our model estimates of LGM cooling differ by 3.4 °C from CLIMAP in the eastern equatorial Pacific (where CLIMAP suggests slight warming), dropping to about 1 °C in the western equatorial Pacific. The Indian and Atlantic equatorial oceans are 1–2 °C lower than CLIMAP estimates, in line with recent alkenone measurements^{3,4,6,35}. Our discrepancy with CLIMAP is less in the Northern Hemisphere summer, where our model is in fact up to 1.8 °C warmer than CLIMAP in the warm pool of the western equatorial Pacific.

The weakening and shallowing of the North Atlantic conveyor in the LGM experiment and the general surface cooling caused a redistribution of water masses in the ocean as indicated in Fig. 5. Model results suggest only a slight cooling (~0.2 °C) of AABW near the source region, with a larger (~0.5–0.7 °C) general cooling of the deep ocean, and an even larger (~1.5–3.5 °C) cooling in the thermocline waters (Fig. 5a). In the Atlantic (Fig. 5b), the cooling is pronounced in the region of NADW export to the Southern Ocean, due to a reduction of the conveyor (Fig. 1b).

Sensitivity to components of radiative forcing

We now determine the extent to which the response found in the last section is due to orbital forcing, CO₂ forcing, ice-sheet albedo feedback, or the wind-stress feedback parametrization. Four additional experiments were performed which involved repeating the LGM experiment with a particular process turned on or off. In the first of these four experiments, the ice-sheet albedo feedback was turned off. The thermohaline circulation still weakened under the combined effects of orbital and atmospheric CO₂ forcing, although the global mean SAT and SST were now only 2.5 °C and 1.8 °C cooler than the present, respectively. This shows that the addition of the albedo feedback accounted for about 0.7 °C and 0.5 °C of the global mean SAT and SST cooling, respectively, although as discussed later, the role of ice-sheet albedo feedbacks may be underestimated in our model. The spatial pattern of the difference clearly showed intensified cooling over the locations of the Laurentide, Fennoscandian and Antarctic ice sheets which in turn caused diffusive heat transport from the oceans to land and subsequent SST cooling.

We now use the results of the experiment without the ice-sheet

albedo feedback as the reference to examine the sensitivity to other feedbacks. The removal of the wind stress feedback had little effect on the climate response, although there were small local changes in the North Atlantic where the feedback was strongest. When the orbital forcing was turned off (by setting orbital parameters to present-day values) the resultant annual-mean response of the model was almost identical to the response with it included, although the seasonal variation in SAT was increased. Global-mean SAT and SST were now 2.5 °C and 1.9 °C cooler than the present, respectively. These numbers are virtually the same as those reported with no ice-sheet albedo feedback.

When the atmospheric CO₂ forcing was turned off, leaving the orbital parameters at values for 21 kyr ago, there was only a slight cooling from the present day in the annual and global mean SAT (0.4 °C) and SST (0.1 °C). This slight cooling was caused by an enhanced ice albedo feedback which existed in high latitudes, as more sea-ice was present in the summer due to a decreased seasonal variation in SAT. Nevertheless, the reason why the previous experiment (with no orbital forcing) captures the global mean SST and SAT cooling response found when both orbital and CO₂ forcing are included, is that the small changes in sea-ice extent due to the reduced seasonal cycle are encompassed within the larger changes in sea-ice extent due to the changes in atmospheric CO₂.

Sensitivity to initial present-day conveyor strength

Two studies^{42,43} have demonstrated the potential instability of the North Atlantic conveyor in ocean GCMs when the overturning rate is near a stability threshold. We examine this in our model by conducting a series of experiments, identical to those described in the previous two sections, but now with slightly different initial present-day conveyor strengths. It is well known⁴⁴ that the strength of the conveyor is very sensitive to the amount of freshwater discharge into the North Atlantic. In addition, a significant uncertainty in our model concerns what river drainage basins should be imposed, as we have no topography on land and hence precipitation is not induced by topographical features such as mountain ranges. Therefore, to accomplish the task of creating several initial strengths of the conveyor, we modified the catchment areas of a few rivers

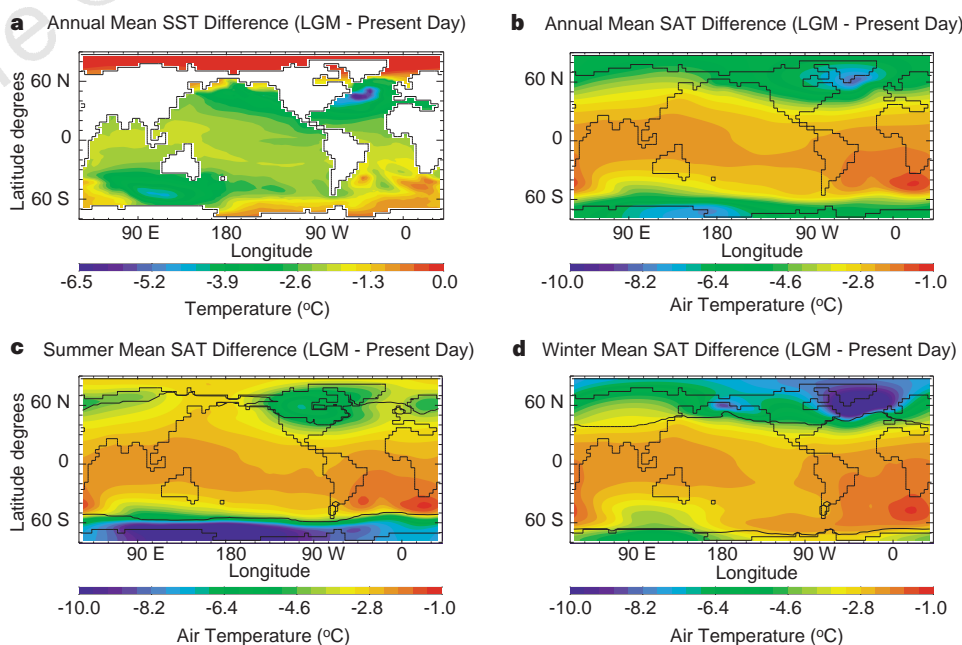


Figure 3 Difference fields between the LGM and present-day experiments. **a**, Annual mean SST; **b**, annual mean SAT; **c**, Northern Hemisphere summer SAT; **d**, Northern Hemisphere winter SAT. The black line over the ocean in **c** and **d** indicates the maximum sea-ice extent whereas on land it indicates the latitude of

the –10 °C contour or the ice-sheet boundary (whichever extends further equatorward). By showing sea-ice extent averaged over a season, the contour will show the maximum sea-ice extent during that time. The minimum extent in summer is further north than indicated in **c**.

around the North Atlantic, thereby changing the amount of fresh-water discharge into the ocean there.

The modifications that were done are illustrated in Fig. 1b. In model 0, the main change was an increase of the Rhine catchment area (over model 1) at the expense of the Amur and Yangtze-Yellow rivers. This had the effect of diverting more fresh water into the North Atlantic instead of the Pacific, with the result that the conveyor had a strength of 12 Sv at the present-day equilibrium (Fig. 6a). When LGM forcing was used with the model 0 drainage basins, a collapse of the conveyor (Fig. 6b) and hence North Atlantic heat transport (Fig. 6c) ensued. In model 2, the Rhine catchment area was decreased slightly from that of Fig. 1a by increasing the discharge into the Amur and Yangtze-Yellow rivers. The net result was a slightly stronger conveyor (now 17 Sv; Fig. 6d) although AABW was beginning to disappear in the deep North Atlantic. The changes made in model 3 involved a more drastic further reduction of the Rhine and increase of the Amur basins. This led to a further increase in the present-day conveyor (to about 18 Sv) but the near elimination of deep AABW in the North Atlantic (Fig. 6g). The choice of the model 1 mask over the other three masks is now clear: model 0 yields too weak a NADW signal whereas models 2 and 3 yield too weak an AABW signal. Model 1, on the other hand, gives an NADW strength of 16 Sv, in good agreement with observations⁴⁵, yet not too strong to prevent the intrusion of AABW.

When forcing characteristic of 21 kyr ago was used in both the model 2 and 3 suite of experiments, the results were similar to those of model 1, although differences existed. In particular, the stronger the present-day conveyor was at equilibrium (Figs 2a, 6a, g), the further it was from a stability threshold and so the less sensitive it was to 21-kyr-ago forcing (Figs 2b, 6e, h). In fact, the equilibrium heat transport for the LGM changed less for a stronger present-day conveyor (Figs 2c, 6f, i). This result is more in line with the

assumption used in ref. 20 although convergence was not reached and the present-day thermohaline circulation became less realistic. Indeed in model 3, the Atlantic and hence global heat transport in fact increased under LGM forcing. For all our present-day climatologies, the discussion of CO₂, orbital forcing and ice-sheet feedbacks given in the last section remained valid.

Possibly the most remarkable result is that for all four LGM experiments, starting from four different realizations of the present-day ocean climate, the global-mean SST and SAT cooling at equilibrium were virtually the same (~2.3 and ~3.2 °C, respectively), although significant regional differences existed. Tropical SST differences averaged over the latitude band 20° S to 20° N were also the same in these four experiments (2.2 °C cooling). This suggests that redistributions in ocean circulation did not cause enhanced global mean cooling in the LGM unless they did so indirectly, via changes in CO₂ release/uptake. This is in contrast with results in ref. 22 where a 30% contribution to global cooling was found, due to a reorganization of the ocean circulation. This discrepancy may be due to the more southward LGM sea-ice extent in ref. 22 (and the subsequent ice-albedo feedback) due to a southward shift in the location of NADW formation. In addition, the lack of an ocean feedback contributing to enhanced global cooling accounts for most of the difference in LGM cooling between results of ref. 22 and our results.

Interpretations and implications

Although our EMBM is admittedly idealized, the present study represents an attempt to examine quantitatively the climate of the

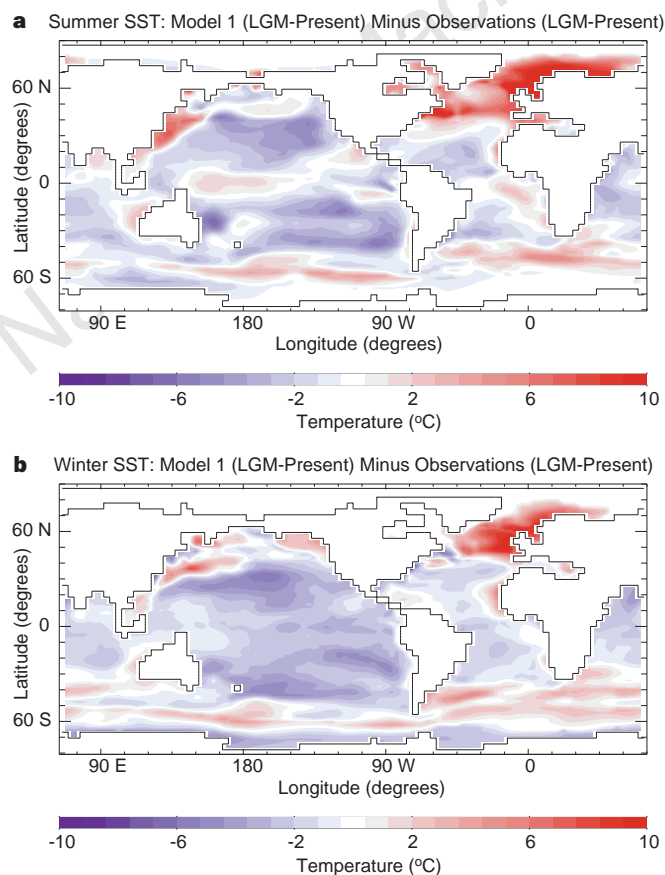


Figure 4 Anomaly maps showing the difference between model and CLIMAP¹² SST changes between the LGM and the present day. **a**, Summer; **b**, winter.

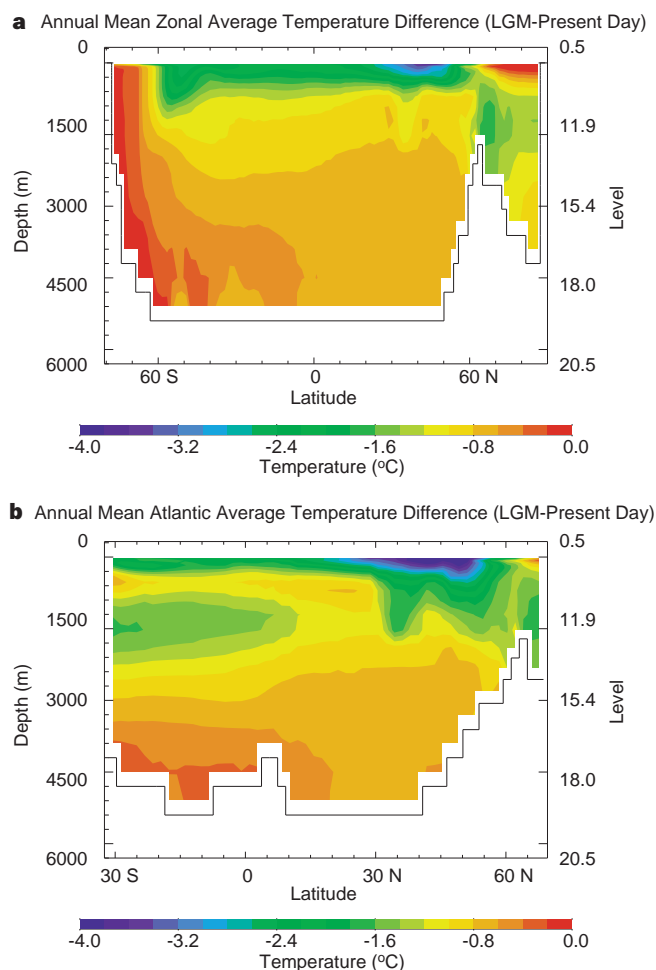


Figure 5 Zonally averaged ocean potential temperature difference fields between the LGM and present-day experiments. **a**, Global average; **b**, Atlantic average. The model level corresponding to the depth is given on the right-hand y-axis.

LGM and its sensitivity to ice-sheet albedo, orbital forcing and atmospheric CO₂ using a coupled model which is integrated to equilibrium. Our experiments were purposely kept simple in order to try and reveal the competing effects of the different forcing mechanisms. We have not included the radiative forcing associated with atmospheric aerosols for a number of reasons. First, it is not clear what the spatial pattern of this aerosol forcing would be in terms of both aerosol type and distribution. For example, estimates from Peru⁹ suggest that LGM atmospheric dust levels may have been 200 times the present, whereas in Antarctica they may have been 4–6 times the present for marine and 10–30 times the present for continental aerosols⁴⁶. In addition, it is not clear whether these aerosols would contribute to local cooling or warming through the competing effects of increased albedo and longwave absorption.

The comparison between model results and proxy data over land is complicated by the fact that there is no topography in our EMBM. We would therefore expect, through purely adiabatic cooling, our results over land to be warmer than those in the proxy record at higher elevations. This follows since latent-heat release in a warmer climate would tend to yield a generally smaller globally averaged adiabatic lapse rate than in a colder climate, due to the nonlinearity of the Clausius–Clapyeron equation. In addition, vegetation feedbacks and subsequent albedo changes through the expansion of dry-land vegetation in Australia and Africa, and the conversion of conifer to tundra in Europe and Siberia, would enhance the cooling there¹⁹. Other potentially important factors were not included in this model; we used the present-day land boundaries which did not account for the sea level drop of 121 ± 5 m (ref. 47) (and hence global mean salinity increase) in the LGM, and the atmospheric model did not allow for changes in cloud cover. We purposely retained the present-day land boundaries in the LGM experiments

to facilitate comparison with model results from the present-day experiment, although additional experiments not presented here with a 120-m sea-level drop accounted for, and with the global mean salinity increased by 1 p.s.u., revealed virtually no differences. In addition, the retention of present-day land boundaries makes easier the understanding of the competing effects of orbital, atmospheric CO₂, and ice-sheet albedo effects. Reduced LGM cloud cover¹⁶ in a drier atmosphere probably contributed to extra cooling, although the incorporation of this effect in our vertically averaged EMBM would be difficult, and perhaps inconsistent with its level of sophistication. In addition, the lack of topography on land does not allow us to capture the topographical effects of ice sheets, which have been shown to act as a summer heat sink (through local melting) and to influence the atmospheric circulation causing the advection of very cold air across the North Atlantic¹⁵. Our reduction of the planetary co-albedo by only 0.1 is also probably an underestimate for the ice albedo. This may explain why CO₂ is a more effective mechanism for cooling in our model, in distinction to the results of ref. 37 where it is of equal importance with ice-sheet effects.

With these shortcomings recognized, a number of conclusions can be drawn from this study. First, the assumption of invariant ocean heat transports between the LGM and the present²⁰ is not consistent with our findings. Second, in response to LGM radiative forcing we found a weakening and shallowing (but not collapse) of the North Atlantic conveyor, consistent with observations^{48,49}. Our model SSTs are in good agreement with alkenone reconstructions^{3–6,34–36}, and are generally cooler than those of CLIMAP^{1,2} in the tropical ocean, while in the North Atlantic, our model results suggest a maximum SST cooling of $\sim 6.3^\circ\text{C}$ with most of the cooling in the $4^\circ\text{--}6^\circ\text{C}$ range (noticeably lower than CLIMAP^{1,2}

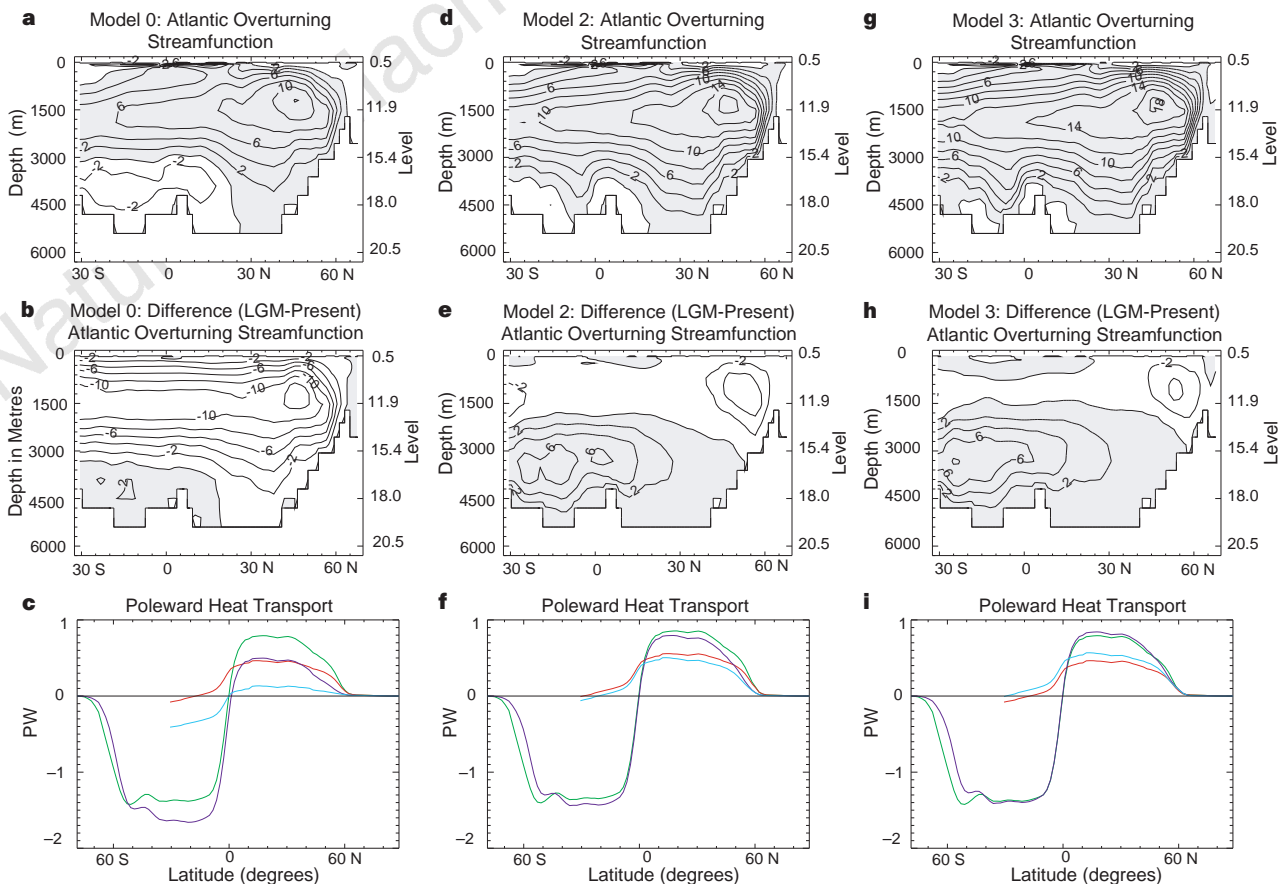


Figure 6 As in Fig. 2 but for the three other experiments with different initial present-day conveyor strengths in the North Atlantic. The drainage basins used to derive the different initial conditions, for the purpose of the sensitivity analysis,

are described in Fig. 1. Model 0 (a–c) gives a weak initial conveyor (12 Sv); model 2 (d–f) and model 3 (g–i) yield stronger initial conveyor strengths than shown in Fig. 2a (17 Sv and 18 Sv, respectively).

estimates). Some of this reduced cooling may be due to our present-day climatology already being slightly colder than observations in the Nordic seas, a problem that is common in coarse-resolution ocean GCMs. Large differences from CLIMAP also exist in the subtropical gyres of all oceans.

For all our LGM experiments starting from different present-day initial conditions, the global-mean SST and SAT cooling at equilibrium were virtually the same, although significant regional differences existed. This result is important, in that it suggests that redistributions in ocean circulation did not directly cause global mean cooling in the LGM, although indirect effects via changes in CO₂ release/uptake are still plausible. The examination of the relative importance of orbital forcing, atmospheric CO₂ levels and ice-sheet albedo feedbacks suggests that the most important of these forcings in our model is the change in atmospheric CO₂, with ice-sheet albedo feedbacks contributing to further cooling. Nevertheless, changes in orbital forcing, through decreased seasonality, do induce slight expansions in sea-ice extent.

Three studies have now been conducted with dynamical ocean models coupled to atmospheric models of various degrees of complexity. In the first of these²², a coarse resolution, zonally averaged ocean model was coupled to a simple dynamical atmospheric model and integrated to equilibrium; in the second²¹, ocean and atmospheric GCMs were coupled together and integrated under LGM forcing for 15 years (starting from a present-day initial condition). The present study (the third) involves the integration to equilibrium of an ocean GCM coupled to an idealized EBM. The climate sensitivity of our model is similar to the model used in ref. 22 (3.0 °C warming upon CO₂ doubling), whereas the GFDL model has a slightly higher sensitivity (3.7 °C)⁵⁰. All three of these studies find tropical temperatures which are colder than CLIMAP^{1,2}, although intermodel differences exist due to the magnitude of the ocean feedback and the sensitivity of each model to its radiative forcing. Our results with low-to-moderate climate sensitivity and no ocean feedback to LGM cooling yield SSTs which are slightly colder than CLIMAP. Ganopolski *et al.*²², once more with a low-to-moderate climate sensitivity, predict cooler tropical temperatures largely through a positive feedback from changes in ocean circulation. Bush and Philander²¹, with a moderate-to-high climate sensitivity, predict cooler tropical temperatures (with global LGM cooling of only 4.3 °C, compared to 3.2 °C here and 6.2 °C in ref. 22). It is possible for us to reconcile a more stable tropics (colder than CLIMAP^{1,2}, consistent with alkenone reconstructions^{3–6}, but not as cold as the bore-hole, coral and other reconstructions^{7–11} mentioned earlier) if the climate sensitivity is low-to-moderate and there is little or no thermohaline feedback. Nevertheless, before such a conclusion is firmly established more effort needs to be directed to understand the following: first, whether or not changes in the ocean circulation can cause a positive feedback on the global-mean LGM cooling via changes in deep and intermediate water production²² or extratropical subduction²¹; second, what the sensitivity is of the real climate system, and how the parametrization of the physical processes of cloud and water-vapour feedbacks affects this climate sensitivity. □

Received 5 December 1997; accepted 29 May 1998.

1. CLIMAP Project Members The surface of the ice-age earth. *Science* **191**, 1131–1137 (1976).
2. CLIMAP Project Members Seasonal reconstructions of the earth's surface at the glacial maximum. (Map Chart Ser. MC-36, Geol. Soc. Am., Boulder, CO, 1981).
3. Sikes, E. L. & Keigwin, L. Equatorial Atlantic sea surface temperature for the last 30 kyr: A comparison of U₃₇, δ¹⁸O and foraminiferal assemblage temperature estimates. *Paleoceanography* **9**, 31–45 (1994).
4. Bard, E., Rostek, F. & Sonzogni, C. Interhemispheric synchrony of the last deglaciation inferred from alkenone palaeothermometry. *Nature* **385**, 707–710 (1997).
5. Lyle, M. W., Prah, F. G. & Sparrow, M. A. Upwelling and productivity changes inferred from a temperature record in the central equatorial Pacific. *Nature* **355**, 812–815 (1992).
6. Rostek, F. *et al.* Reconstructing sea surface temperature and salinity using δ¹⁸O and alkenone records. *Nature* **364**, 319–321 (1993).
7. Guilderson, T. P., Fairbanks, R. G. & Rubenstone, J. L. Tropical temperature variations since 20,000 years ago: modulating interhemispheric climate change. *Science* **263**, 663–665 (1994).
8. Beck, J. W. *et al.* Abrupt changes in early Holocene tropical sea surface temperature derived from coral records. *Nature* **385**, 705–707 (1997).

9. Thompson, L. G. *et al.* Late glacial stage and Holocene tropical ice core records from Huascáran, Peru. *Science* **269**, 46–50 (1995).
10. Stute, M. *et al.* Cooling of tropical Brazil (5 °C) during the last glacial maximum. *Science* **269**, 379–383 (1995).
11. Curry, W. B. & Oppo, D. W. Synchronous high-frequency oscillations in tropical sea surface temperatures and North Atlantic deep water production during the last glacial cycles. *Paleoceanography* **12**, 1–14 (1997).
12. Lautenschlager, M., Mikolajewicz, U., Maier-Reimer, E. & Heinze, C. Application of ocean models for the interpretation of atmospheric general circulation model experiments on the climate of the Last Glacial maximum. *Paleoceanography* **7**, 769–782 (1992).
13. Fichetef, T., Hovine, S. & Duplessy, J.-C. A model study of the Atlantic thermohaline circulation during the last glacial maximum. *Nature* **372**, 252–255 (1994).
14. Winguth, A. M. E. *et al.* On the Sensitivity of an Ocean General Circulation Model to Glacial Boundary Conditions (Rep. No. 203, Max-Planck-Institut für Meteorologie, Hamburg, 1996).
15. Manabe, S. & Broccoli, A. J. The influence of continental ice sheets on the climate of an ice age. *J. Geophys. Res.* **90**, 2167–2190 (1985).
16. Hansen, J. *et al.* in *Climate Processes and Climate Sensitivity* 130–163 (Geophys. Monogr. 29, Am. Geophys. Union, Washington DC, 1984).
17. Lautenschlager, M. & Herterich, K. Atmospheric response to ice age conditions: climatology near the earth's surface. *J. Geophys. Res.* **95**, 22547–22557 (1990).
18. Kutzbach, J. E. & Guetter, P. J. The influence of changing orbital parameters and surface boundary conditions on climate simulations for the past 18000 years. *J. Atmos. Sci.* **43**, 1726–1759 (1986).
19. Crowley, T. J. & Baum, S. K. Effect of vegetation on an ice-age climate model simulation. *J. Geophys. Res.* **102**, 16463–16480 (1997).
20. Webb, R. S. *et al.* Influence of ocean heat transport on the climate of the Last Glacial Maximum. *Nature* **385**, 695–699 (1997).
21. Bush, A. B. G. & Philander, S. G. H. The role of ocean-atmosphere interactions in tropical cooling during the Last Glacial Maximum. *Science* **279**, 1341–1344 (1998).
22. Ganopolski, A., Rahmstorf, S., Petoukhov, V. & Claussen, M. Simulation of modern and glacial climates with a coupled global model of intermediate complexity. *Nature* **391**, 351–356 (1998).
23. Fanning, A. F. & Weaver, A. J. An atmospheric energy-moisture balance model: climatology, interpentadal climate change, and coupling to an ocean general circulation model. *J. Geophys. Res.* **101**, 15111–15128 (1996).
24. daSilva, A. M., Young, C. C. & Levitus, S. *Atlas of Surface Marine Data 1994* Vol. 3 (NOAA, Washington DC, 1994).
25. Fanning, A. F. & Weaver, A. J. Temporal geographical meltwater influences on the North Atlantic Conveyor: Implications for the Younger Dryas. *Paleoceanography* **12**, 307–320 (1997).
26. Semtner, A. J. A model for the thermodynamic growth of sea ice in numerical investigations of climate. *Phys. Oceanogr.* **6**, 379–389 (1976).
27. Thompson, S. J. & Warren, S. G. Parameterization of outgoing infrared radiation derived from detailed radiative calculations. *J. Atmos. Sci.* **39**, 2667–2680 (1982).
28. Graves, C. E., Lee, W. H. & North, G. R. New parameterizations and sensitivities for simple climate models. *J. Geophys. Res.* **98**, 5025–5036 (1993).
29. Peltier, W. R. Ice age paleotopography. *Science* **265**, 195–201 (1994).
30. Pacanowski, R. C. Momz user's guide and reference manual (GFDL Ocean Group Tech. Rep. No. 3, GFDL/NOAA, Princeton, NJ, 1995).
31. Weaver, A. J. & Hughes, T. M. C. On the incompatibility of ocean and atmosphere models and the need for flux adjustments. *Clim. Dyn.* **12**, 141–170 (1996).
32. Berger, A. L. Long term variations of daily insolation and Quaternary climatic changes. *J. Atmos. Sci.* **35**, 2362–2367 (1978).
33. Ramanathan, V. *et al.* Climate-chemical interactions and effects of changing atmospheric trace gases. *Rev. Geophys.* **25**, 1411–1482 (1987).
34. Ikehara, M. *et al.* Alkenone sea surface temperature in the Southern Ocean for the last two deglaciations. *Geophys. Res. Lett.* **24**, 679–682 (1997).
35. Schneider, R. R., Müller, P. J. & Ruhland, G. Late Quaternary surface circulation in the east equatorial South Atlantic: Evidence from alkenone sea surface temperatures. *Paleoceanography* **10**, 197–219 (1995).
36. Chapman, M. R. *et al.* Faunal and alkenone reconstructions of subtropical North Atlantic surface hydrography and paleotemperature over last 28 kyr. *Paleoceanography* **11**, 343–357 (1996).
37. Broccoli, A. J. & Manabe, S. The influence of continental ice, atmospheric CO₂, and land albedo on the climate of the last glacial maximum. *Clim. Dyn.* **1**, 87–99 (1987).
38. Hyde, W. T. *et al.* Comparison of GCM and energy balance model simulations of seasonal temperature changes over the past 18,000 years. *J. Clim.* **2**, 864–887 (1989).
39. Denton, G. H. & Hughes, T. J. (eds) *The Last Great Ice Sheets* (Wiley, New York, 1981).
40. Cooke, D. W. & Hays, J. D. in *Antarctic Geoscience* (eds Craddock, C. *et al.*) 1017–1025 (Univ. Wisconsin Press, Madison, 1982).
41. Hebbin, D. *et al.* Moisture supply for northern ice-sheet growth during the Last Glacial Maximum. *Nature* **370**, 357–359 (1994).
42. Rahmstorf, S. Bifurcations of the Atlantic thermohaline circulation in response to changes in the hydrological cycle. *Nature* **378**, 145–148 (1995).
43. Tziperman, E. Inherently unstable climate behaviour due to weak thermohaline ocean circulation. *Nature* **386**, 592–595 (1997).
44. Maier-Reimer, E. & Mikolajewicz, U. in *Oceanography* (eds Ayala-Castanares, A. *et al.*) 87–99 (UNAM Press, Mexico, 1989).
45. Schmitz, W. J. Jr On the interbasin-scale thermohaline circulation. *Rev. Geophys.* **33**, 151–173 (1995).
46. Petit, J. R., Briat, M. & Royer, A. Ice age aerosol content from East Antarctic ice core samples and past wind strength. *Nature* **293**, 391–394 (1981).
47. Fairbanks, R. G. A 17,000-year glacial-eustatic sea level record: Influence of glacial meltwater rates on Younger Dryas event and deep ocean circulation. *Nature* **342**, 637–642 (1989).
48. McIntyre, A. *et al.* in *Investigations of Late Quaternary Paleoclimatology and Paleoclimatology* (eds Cline, R. M. & Hays, J. D.) 43–76 (Geol. Soc. Am., Boulder, CO, 1976).
49. Boyle, E. & Keigwin, L. D. North Atlantic thermohaline circulation during the past 20,000 years linked to high-latitude surface temperature. *Nature* **330**, 35–40 (1987).
50. Kattenberg, A. *et al.* in *Climate Change 1995; the Science of Climate Change* (eds Houghton, J. T. *et al.*) 285–357 (Cambridge Univ. Press, 1996).

Acknowledgements. All numerical computations were conducted locally on a suite of IBM RS6000s including two SP2s. We thank S. Rahmstorf and T. Stocker for comments on an earlier version of this manuscript, and A. Broccoli for a review which significantly improved the manuscript. This work was supported by NSERC, CSHD, CICS, NOAA and Steacie operating grants, as well as an IBM SUR grant.

Correspondence and requests for materials should be addressed to A.J.W. (e-mail: weaver@ocean.seos.uvic.ca).